Band structure treatment of the influence of nonstoichiometric defects on optical properties in LiNbO3

ARTICLE *in* JOURNAL OF APPLIED PHYSICS · NOVEMBER 2001

Impact Factor: 2.18 · DOI: 10.1063/1.1413942

5 AUTHORS, INCLUDING:

Iwan V Kityk
Czestochowa University of Technology
959 PUBLICATIONS **7,927** CITATIONS
SEE PROFILE

Malgorzata Makowska-Janusik
Akademia Jana Dlugosza w Czestochowie
104 PUBLICATIONS **944** CITATIONS
SEE PROFILE

Marc D Fontana
University of Lorraine
297 PUBLICATIONS **2,336** CITATIONS
SEE PROFILE

M. Aillerie
University of Lorraine
253 PUBLICATIONS **1,008** CITATIONS
SEE PROFILE

Band structure treatment of the influence of nonstoichiometric defects on optical properties in $LiNbO_3$

I. V. Kityk[a] and M. Makowska-Janusik
Institute of Physics WSP, PL-42201, Al.Armii Krajowej 13/15, Częstochowa, Poland

M. D. Fontana, M. Aillerie, and F. Abdi
Laboratoire Materiaux Optiques à Proprietes Specifiques, CLOES, University of Metz, and Supelec, 2 rue Ed. Belin, 57070 Metz Cedex, France

(Received 14 February 2001; accepted for publication 4 September 2001)

We present a band structure approach in connection with a molecular dynamics cluster optimization that accounts for various structural modifications related to the nonstoichiometry of $LiNbO_3$ crystals. Variation of optical properties with the deviation from the stoichiometric composition can be understood within this approach. The particular role of the electron-phonon contributions to the electro-optic coefficient is shown. Model calculations yield a large dependence of the electro-optic coefficient r_{22} on the crystal composition, in agreement with the experimental data. The observed minimum of the r_{22} coefficient versus nonstochiometry is explained within a microscopic approach. The r_{33} tensor component shows substantially different behavior versus the stoichiometry. © *2001 American Institute of Physics.* [DOI: 10.1063/1.1413942]

I. INTRODUCTION

It was recently reported that optical properties of pure $LiNbO_3$ (LN) crystals are sensitive to the presence of the intrinsic defects related to the nonstoichiometry of the crystals.[1] Furthermore, the electro-optic[2] and nonlinear optical properties[3] are also strongly dependent on the concentration of these intrinsic defects. This can lead to some problems in the use of LN crystals in technological applications. It is therefore of considerable importance to control the real composition of the crystal, or its deviation from the stoichiometry.

The parameter X_c, is defined as a ratio of the Li content and the total amount of cations (Li+Nb) and is introduced to characterize the deviation from the stoichiometry. The $X_c = 48.6\%$ is the composition in the congruent crystal whereas $X_c = 50\%$ corresponds to the stoichiometric composition. Various methods have been proposed to determine the crystal composition X_c (Ref. 4). Among them, the calibration of crystals from measurements of the refractive index,[4] the absorption band edge,[5] or the Raman phonon linewidth.[6] Up to now, no theoretical investigations on calculations are available that are based on the microscopic band energy approach.

All the previous considerations of the nonlinear optical susceptibilities in congruent LN were based on a phenomenological bond length approach.[2,7] However in the case of LN single crystals neglecting of the long order crystalline band structure contributions to the susceptibilities could lead to an essential error in determining how much local rearrangements contribute to the nonlinear optical coefficient. Recently,[2,8] it was shown[3,9] that stoichiometric pure LN crystal long-range interactions give a contribution at least 16% due to electronic and about 9% due to phonon subsystems. An oversimplified cluster approach to evaluate the nonlinear optical susceptibility and the long-range contributions.

Such an approach could be partially suitable for an ideal (perfect) crystal but it is absolutely insufficient for doped crystals. We will consider the band energy for the perfect (pure stoichiometric) crystal and then take into account existing defect states. The latter can be considered as a modulation of the ideal crystalline structure by the long-range defect fields. We suppose that the Nb atoms substitute Li ions on the so-called Nb antisites and as a consequence we have local structural rearrangement with creation of the near-the-Li oxygen vacancies and Nb_{Li} antisites. Afterwards we evaluate spectral dependencies of the imaginary part of the dielectric susceptibility $\varepsilon_2(E)$ versus the parameter X_c and determine particular contributions of the different clusters to the $\varepsilon_2(E)$. The similar approach has been just successfully applied to the disordered materials: glasses,[10] guest-host polymers,[11] complex, and doped crystals.[12] The investigated LN crystal can be considered as slightly disordered crystals.[13–23] As a consequence, the approach mentioned may be used. For an explanation of optical spectra and particularly of nonlinear optical properties a better agreement between theory and experiment has been achieved using norm-conserving pseudopotential (NCPP) method because the optical effects are determined first of all by the external valence electrons and unoccupied excited states. Unfortunately, self-consistent eigenenergy convergence within a framework of one-electron band structure approach is not appropriate for performing of the molecular dynamics structure optimization. Thus an additional molecular dynamics procedure is necessary. For the second-order nonlinear optical effects (particularly, for the optical second harmonic generation), contrary to the usual optical effects, the noncentrosymmetry in the charge density distribution plays a key role,[14,15] contrary to the case of the usual optical effects. Therefore an

[a]Electronic mail: i.kityk@wsp.czest.pl

appropriate connection of the solid state approach with the local structure optimization will be applied. Furthermore, for the linear electro-optics substantial contribution gives phonon subsystems.

The main principles of our approach are the following: band energy structure calculations of the LN using self-consistent norm conserving pseudopotential method for the perfect and nonstoichiometric samples; determination of optical constants depending on the degree of nonstoichiometry; evaluations of the $(Nb-O_6)$ intracluster charge density distribution without and with taking into account of the molecular dynamics structure simulations. Simulation of the electro-optic tensor components dependencies versus the nonstoichiometry with taken into account of the electron and phonon subsystems.

Band energy structure of the LN crystals versus the composition X_C in Sec. II is presented. Molecular dynamics procedure and the structure optimization are reported in Sec. III. Structural rearrangements of particular clusters are simulated depending on the nonstoichiometry. In Sec. IV the phonon contributions to the electro-optic coefficient r_{22} are calculated for the crystals with various compositions. Particular contributions of the UV-electronic states modified by effective electron–phonon interactions are presented in the Sec. V. Discussion concerning agreements and discrepancies between the proposed approaches and the experimental data is carried out.

II. BAND STRUCTURE OF LN CRYSTALS WITH INTRINSIC DEFECTS

Up to now there is only one work devoted to *ab initio* band structure calculations of the LN single crystals[15] that are in agreement with the experimental x-ray photoelectron spectra.[16] As a more efficient method of the band energy calculations for such kinds of systems seems to be the NCPP calculation method.[17]

In this article, we perform a detailed calculation of the band electronic structure and of the appropriate optical properties of the LN crystals using the self-consistent NCPP method (DFT).[21] This method was also verified during calculations of the nonlinear optical properties of complex systems,[8,18] metallic glass systems,[21] polymer-like systems,[22] etc.

The total energy may be expressed within a framework of the local density functional approach:

$$E_{\text{tot}}[\rho(r)] = T[\rho(r)] + V_{n-e}[\rho(r)] + V_{e-e}[\rho(r)] + V_{e-c}[\rho(r)], \tag{1}$$

with

$$\rho(r) = \Sigma_{\beta,1} |\Psi(1,\mathbf{r},\beta)|^2. \tag{2}$$

Kinetic energy function $T[\rho(r)]$ is calculated as a functional of the electron charge density $\rho(r)$; $V_{e-e}[\rho(r)]$, and $V_{e-c}[\rho(r)]$ are screening potentials corresponding to electron–electron and exchange–correlation interactions, respectively. $V_{n-e}[\rho(r)]$ corresponds to nuclear–electron Coulomb-like interaction that in this article is chosen in the form described in Ref. 17. A nonlinear extrapolation procedure was conducted in the form convenient for the analytical evaluations (Gaussian-polynomial-like):

$$V_{n-e}^{(\beta,l)} = \sum_i \left[A_i^\beta + r^2 A_{i+3}^\beta \exp(-\alpha_n^{(l,\beta)} r^2)\right] \tag{3}$$

where β denotes the kind of atom; l is an angular momentum; value of n depends on the precision of fitting procedure. During the nonlinear interpolations the NCPP has been expressed in form of at least 18 Gaussian-polynomial orbitals with decaying exponents is equal to 0.001–835 000. The basic wave functions consisted of $1s-5d$ orbitals of Nb, $1s-3p$ orbitals of Li, and $1s-4s$ orbitals of O. We have also included excited orbitals to enhance the precision of the matrix dipole momenta. The proposed approach is allowed to achieve the eigenvalue convergence up to 0.0013 eV. Coefficients a and α were fitted using the nonlinear extrapolation procedure.

Detailed expressions for the corresponding matrix elements are presented in the Refs. 11 and 12. The procedure solve the following secular equation:

$$\left\| \left[\frac{h^2(\mathbf{k}+\mathbf{G}_{n,n'})^2}{2m} - E(\mathbf{k}) \right] \delta_{n,n'} + \sum_\alpha V_\alpha(\mathbf{G}_n' - \mathbf{G}_n) \times S_\alpha(\mathbf{G}_n' - \mathbf{G}_n) \right\| = 0, \tag{4}$$

where $E(\mathbf{k})$ is the searched eigenenergy for a given $\mathbf{k}$ point of the BZ; $\mathbf{G}_n'$ and $\mathbf{G}_n$ are interacting basis plane waves. For the stoichiometric samples we have taken at least 3680 plane waves and additional 1244 plane waves with the Lowdin approximation. As a criterion of the convergence the stability of the eigenenergies within the 0.0015 eV was chosen. For the nonstoichiometric case we have taken at least 4286 and 1346 basis plane waves, respectively. Increase of the convergence limit from 0.02 eV up to 0.002 eV causes maximal shift of the particular eigenenergies less than 0.04 eV that corresponds to the changes of the matrix dipole moments below 8.2%.

Solving of the mentioned secular equations was carried out using the (Querry Ltd.) QL-modified Jacobi method. The structural factor for the β kind of atom was evaluated in the form:

$$S_\beta^{(\alpha)}(\mathbf{G}_n' - \mathbf{G}_n) = \frac{g^{(\alpha)}}{N\Omega} \sum_\beta \exp[-i(\mathbf{G}_n' - \mathbf{G}_n)\boldsymbol{\tau}_\beta], \tag{5}$$

where τ_β denotes position of the βth atom. Here $g^{(\alpha)}$ corresponds to the particular contributions of the αth ions and is determined by stoichiometry of composition. Varying the weighting coefficients $g^{(\alpha)}$ the band energy structures for the given nonstoichiometry was obtained. This procedure for particular cases of vacancy-induced states and solid alloys is described in the Refs. 12 and 18.

Fourier transformations of the pseudopotential for the αth kinds of ions take a form:

$$V_\alpha^{(\alpha)}(\mathbf{G}_n' - \mathbf{G}_n) = \frac{1}{\Omega} \int V^{(\alpha)}(r) \exp[-i(\mathbf{G}_n' - \mathbf{G}_n)\tau_\beta] d^3r. \tag{6}$$

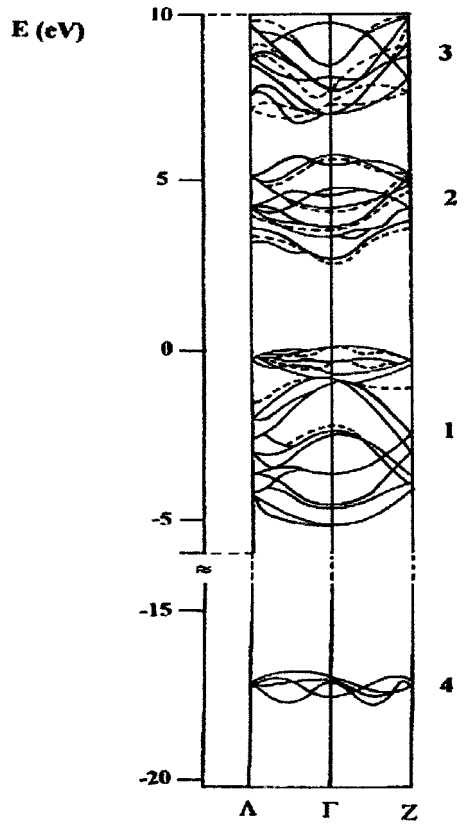

FIG. 1. Band structure of the LN crystals for the $X_C = 48.4\%$. Main deviations from bands of the perfect LN crystals are indicated by dashed lines.

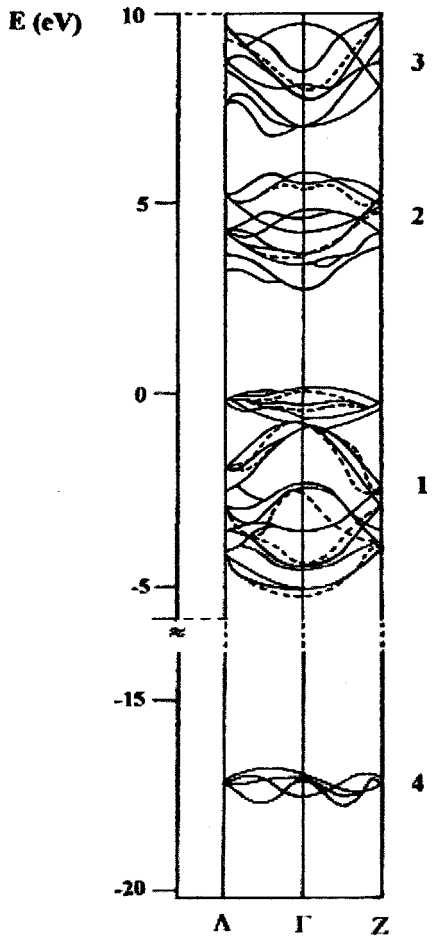

FIG. 2. Same for the $X_C = 48.7\%$.

Electron screening effects were calculated using parameters introduced by Perdew–Zunger[23] and Ceperley–Alder.[24] A special method of Chadhi–Cohen[25] was applied for calculation of the electron charge density distribution. The diagonalization procedure was performed in the 32 special points of the Brillouin zone (BZ) and afterwards an extrapolation was done using a perturbation **kp** method.[26,27]

Acceleration of the iteration convergence was achieved by mixing the $(m-1)$th iteration with the 70% of the output ρ before their substitution into the next equation. A criterion of the self-consistence was satisfied after ensuring the condition:

$$|\rho_{\text{out},m} - \rho_{\text{inp},m}| < \varepsilon, \tag{7}$$

after the mth iteration step. We assumed an accuracy less than $\varepsilon = 8.5\%$ between the input and output iterations as a main criterion of the self-consistency. The searched eigenvalues were stable within a range of 0.002 eV. The numerical evaluations of the charge density function terms were carried out using a numerical tetrahedral method with an increment about 0.002 Hartree.

We started the calculations for the perfect stoichiometric crystals with the factor $g^{(\alpha)}$ equal to 1. Afterwards the factors $g^{(\alpha)}$ have been varied appropriately to the given X_C. Finally we get the band energy structure in the **k** space. All the calculations have been done for the 412 points of the BZ. In Fig. 1 we present two main BZ directions ($\Gamma - Z$ and $\Gamma - \Lambda$), corresponding to parallel and perpendicular directions with respect to the third-order optical axis of the LN single crystals. The band structure was obtained both for stoichiometric and nonstoichiometric samples.

Figures 1–3 present band structures of the LN for the congruent (solid lines) and nonstoichiometric X_C specimens (main deviations are indicated by the dashed lines). Comparing the calculated data with the experimental ones (on the X-ray photoelectron spectroscopy[16]) we revealed an agreement up to 0.17 eV. The value of the calculated energy gap was less than 3.69 eV comparing with 3.80 eV obtained from the absorption edge.[8] Refractive index was equal to 2.1578 that is close to the experimentally measured (2.1397).[2] All these data show that the adopted approach is sufficient for explaining of the main optical parameters. One can clearly see that maximal deviations from the perfect band structure are observed for the $X_C = 48.4\%$. The changes in the energy dispersion and in the absolute values are more clear for the bands (indicated by 1 and 3) originating from the $2p$ O orbitals. This once more confirms that the main changes of the band structure are originated from the delocalized $2p$ O states. The $4d$ Nb states (indicated by the number 2 in the Figs. 1–3) forming the conducting band states are less dependent on the X_C. Core-like $2s$ O band (indicated by the number 4) is independent on the X_C. First of all we should point out an appeared anisotropy of energy dispersion with decreasing X_C that is manifested in different energy disper-

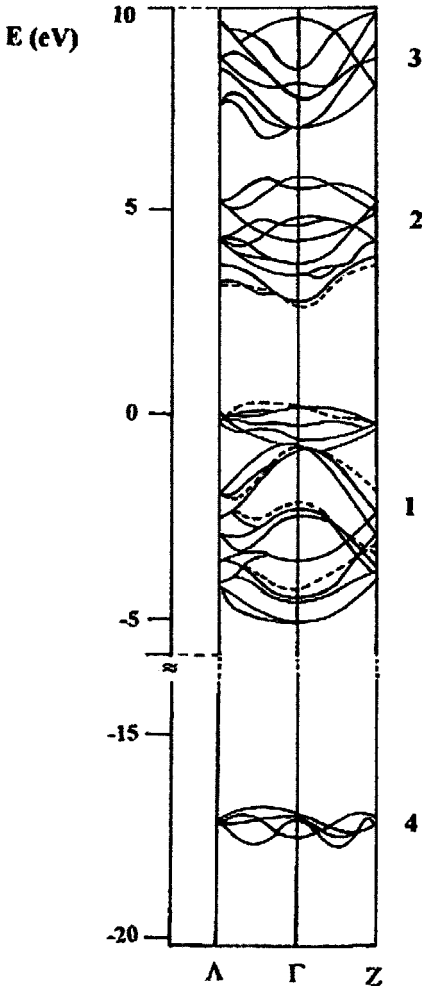

FIG. 3. Same for the $X_C = 49.5\%$.

sion along the $\Gamma - L$ direction of the BZ (perpendicular to the optical axis) and along the $\Gamma - Z$ direction (parallel ones). This is caused by anisotropy in the localization of the corresponding band carriers. The presented data unambiguously indicate that the nonstoichiometry has essential influence on the density of states and on the carrier effective mass determining the band electron localization. The increase of the carrier localization (more flat **k** dependencies) is clearly shown for the $X_C = 48.4\%$. And for the $X_C = 49.5\%$ the localization is very similar to that for the perfect LN crystals. Such complicated dependencies of the band structure localization reflect a competition between the long-range crystalline ordering in the perfect crystals and the local disorder due to the oxygen defect presence. Maximal deviations in the band energy dispersion comparing with calculations in the perfect crystals are equal to 0.22 eV. The performed minimization procedure within a framework of one-electron approach is not appropriate for the total energy evaluation within the particular structural clusters. In the nonstoichiometric LN crystals, likewise in the case of the disordered materials,[9,10] we should do additional molecular dynamics simulations within the particular clusters in order to explain the observed changes of the noncentrosymmetry and of the corresponding electro-optic coefficients described by the third-order polar tensors. Band energy calculations did evalu-

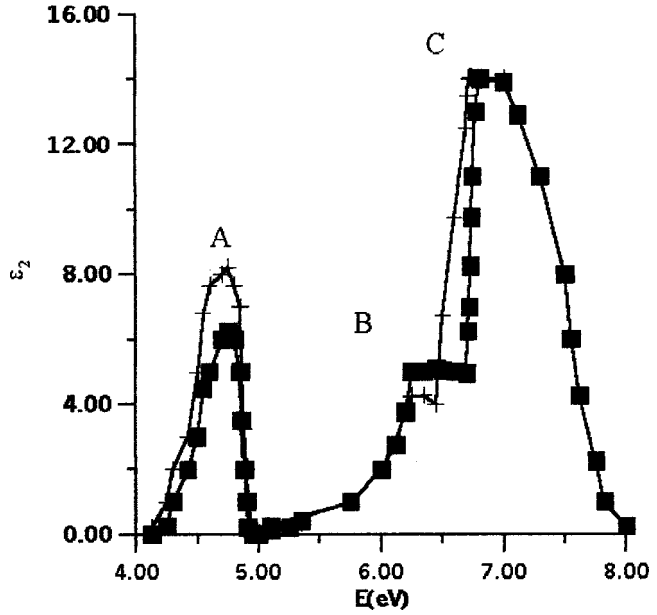

FIG. 4. Two-dimensional representation of imaginary part of the $\varepsilon_2(E)$, as calculated in crystals with various composition X_C. Dashed line: $X_C = 48.7\%$; continuous line: $X_C = 50\%$.

ations of the imaginary part of the $\varepsilon_2(E)$ using the equation:

$$\varepsilon_2(E) = 2\pi N e^2/h^3 \sum_{v.b.\mathbf{k}} \int |\langle \Psi_{v.b} \cdot (\mathbf{k},\mathbf{r}) | \nabla_r \Psi_{c.b} \cdot (\mathbf{k},\mathbf{r}) | \rangle \times d^3\mathbf{r}\, \delta[E_{v.b}(\mathbf{k}) \cdot - E_{c.b}(\mathbf{k}) \cdot - E], \quad (8)$$

where $\Psi_{v.b} \cdot (\mathbf{k},\mathbf{r})$ and $\Psi_{c.b} \cdot (\mathbf{k},\mathbf{r})$ correspond to the valence and conduction band pseudowavefunctions, respectively. The summation is carried out over the whole BZ. Figures 4 and 5 report the spectral calculated dependence of the imaginary part of the $\varepsilon_2(E)$ for the crystals with various compositions. Both two-dimensional as well three-dimensional plots are given. For convenience, the main peaks in the spectral dependencies in Figs. 4 and 5 are indicated by A, B, and C.

Figure 4 exhibits three spectral maxima successively labeled A, B, and C around 4.8, 6.32, and 6.88 eV, respectively. They correspond to the interband optical transition

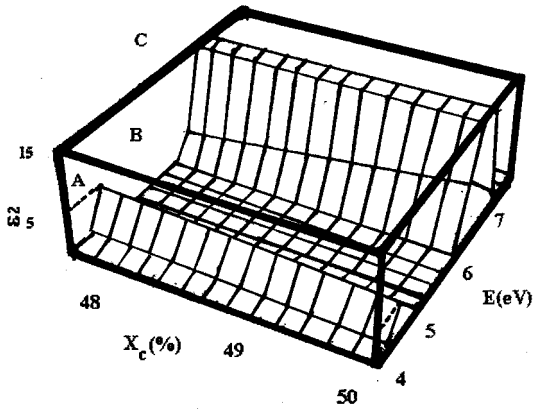

FIG. 5. Three-dimensional representation of $\varepsilon_2(E)$ vs energy E and nonstoichiometry X_C.

TABLE I. Distances between the main ions within the ($Nb–O_6$) clusters before and after the molecular dynamics structure optimization procedure.

N	Before molecular dynamics simulation			After molecular dynamics simulation		
X_C(%)	Nb–O(1) (A)	Nb–O(2) (A)	U_{tot} (eV)	Nb–O(1) (A)	Nb–O(2) (A)	U_{tot} (eV)
48.4	2.321(8)	2.304(7)	−22.12(0.02)	2.333(0.012)	2.269(0.012)	−26.94(0.02)
48.7	2.313(3)	2.294(4)	−19.68(0.02)	2.304(0.012)	2.261(0.012)	−25.75(0.02)
49.5	2.302(1)	2.292(5)	−24.35(0.02)	2.319(0.012)	2.280(0.012)	−27.35(0.02)

oscillators originating from the two structural clusters. Oscillator A′ originates from the intracluster $4d$ Nb–$2p$ O relatively localized states whereas oscillators B and C are caused by the $2p$ O–$2s$ Li states. The intensities of the peaks A, B, and C (see Fig. 5) are changed with varying composition X_C.

The intensity of C is stable and therefore is related to the long-range highly delocalized $2p$ O–$2s$ Li orbitals. Peaks A and B show opposite dependencies versus composition X_c. The exponentially like decrease of the first oscillator with raising X_C reflects the diminishing content of the Nb ions on the Li site (the so-called Nb_{Li} antisites).

The nonlinear increase of the oscillator B can be caused by oxygen-vacancy states since the concentration of the oxygen vacancies decreases with raising X_c simultaneously with increasing Li sites occupation by Li ions. Our calculations (decrease of peak A) are in agreement with the experimental shift of the energy gap with X_c. Increase of convergence limit from 0.02 eV up to the 0.000 42 eV changes the appropriate dipole momenta by less than 9%. Therefore in order to evaluate the observed changes of the optical or electro-optic constants (not the values) versus the crystal composition, it is necessary to carry out the simulations with the convergence limit up to 0.02–0.002 eV.

The presented results indicate that even without the molecular dynamics near-the-defect structural rearrangement can explain the main linear optical effects (absorption, refractive index) as well as the band structure. However, this approach is not sufficient enough for explanation of the electro-optic effects. This problem will be considered in Sec. III. We have also checked that the contributions from oscillators with energies higher than 7.5 eV is independent on crystal stoichiometry.

III. MOLECULAR DYNAMICS SIMULATIONS

In Sec. II we have found that the band structure calculations show opposite behaviors versus the composition X_c for the main optical oscillators, even if the local structural rearrangement is neglected. In this section we will show how the electron contributions influence to the local cluster [NbO_6] or [LiO_6] local density distribution. For this goal, we use molecular dynamics geometry optimization.

As a starting point we have applied Becke's method[26] using the electrostatic potential parameters obtained from the band structure calculations. The main advantages of the method consists of a very fast convergence of the eigenvalues with respect to the size of the basis sets. Geometry optimization for each crystal composition was done using the gradient-corrected potential function in the electrostatic potentials with the step of 0.05%.

The nondynamic correlation was taken into account within the molecular cluster self-consistent functional approach included in the GAMESS program.[9] Geometry optimization was performed using the gradient boundary conditions of the GAMESS program, and the dynamics boundary conditions were used. Afterwards, we calculated the matrix dipole moments. The equilibrium atom positions were determined from a condition of the minimum of the total energy U_{tot}.

We have found that distribution of charge density in (NbO_6) is strongly dependent on the crystal composition, whereas the electrostatic potential around the cluster (LiO_6) was nearly insensitive to changes of X_C. Therefore, only the (NbO_6) clusters have been considered. It is well known also from the simpler approach that these clusters play a key role in the observed effects.

We have found a redistribution of the electrostatic potential around the ($Nb–O_6$) clusters. The performed calculations unambiguously show that the molecular dynamics structure optimization causes additional structural stabilization (lowering of the total energy U_{tot}). Furthermore, the distances Nb–O(1) and Nb–O(2) clearly demonstrates an existence of the noncentrosymmetry. Table I unambiguously shows important role of the additional geometry optimization for obtaining the more stable geometry structure (lower total energy) and the occurrence of the noncentrosymmetry in the electrostatic potential distribution. The latter also confirms the conclusion done for the disordered materials[9–11,13,14] concerning the necessity of additional total energy optimization within the particular structural clusters to achieve more stable structural conformation.

IV. PHONON CONTRIBUTIONS TO THE ELECTRO-OPTIC COEFFICIENTS

It is well known that taking into account of the phonon subsystem is necessary for calculation of electro-optic coefficients. Therefore in this section we will attempt to evaluate the particular contributions of the phonon modes to the calculated electro-optic coefficient r_{22}. Such an approach was successfully applied for chalcogenide glasses[14] and here is only extended to the slightly disordered crystals (nonstoichiometric LN). We will present prevailing values of electro-optics tensor coefficients r_{ijk} for He–Ne laser line ($\lambda = 0.633$ mm) because this wavelength is more important for technologists creating devices for working in the convenient laser generation range.

The quantum chemistry calculations were performed self-consistently after separation of the electron and phonon contributions. Schrödinger equation for a purely vibration motion was expressed within a harmonic approximation as:

$$d^2\Psi_k/dQ_k^2+(8\pi^2\mu_k h^{-2}\Omega_k-4\pi^2\mu_k h^{-2}\Omega_k^2)\Psi_k=0, \tag{9}$$

where Ψ_k is a wave function corresponding to kth normal coordinate Q_k; μ_k denotes a reduced mass of the nuclei and Ω_k is the eigenfrequency for the kth phonon mode. It is obvious that solutions to the above equation are determined by a model which is responsible for the force constant calculations (so called Hessian matrices), i.e., the second derivatives of an electrostatic cluster potential with respect to given normal coordinates. All the phonon frequencies have been fitted to the existed experimental Raman data.[6]

Besides the usual harmonic modes we have also taken into account the anharmonic electron–phonon interaction potential that was calculated in a nonlinear approximation:[22]

$$V_{e-ph}(\mathbf{r}_i)=e^2\sum_{ms} M_{ms}^{-1/2}\left[Z_{ms}(\mathbf{r}_s-\mathbf{u}_{ms})|\mathbf{r}_s-\mathbf{u}_{ms}|^{-3} - \sum_{m's'} Z_{m's'}(\mathbf{r}_{s'}-\mathbf{u}_{m's'})|\mathbf{r}_{s'}-\mathbf{u}_{m's'}|^{-3}\right] \tag{10}$$

where M_{ms} and eZ_{ms} are the effective ionic mass and charge, the corresponding ions are labeled by m and s, respectively. The $\mathbf{u}_{ms,m's'}$ vector is a relative displacement of two ions from their equilibrium positions $\mathbf{r}_s$ and $\mathbf{r}_{s'}$. Probability of a one-phonon is equal to

$$W(\Omega_k)=4(h/2\pi)^{-2}c^{-3}H^{-1}g^{-1}(\mathbf{r}_i)(E_{el}-\Omega_k)^2B(\Omega_k), \tag{11}$$

where the η and ξ are the lower and upper electron molecular orbital (MO) energy levels, respectively; H is a sum of the η and ξ levels widths, E_{el} is an energy of the interband transitions, Ω_k denotes a kth phonon energy and $g(r_i)$ is a degeneration degree of the corresponding electron energy levels. The parameter $B(\Omega_k)$ is equal to[22]

$$B(\Omega_k)=\sum_{\eta}^{g(\eta)}\sum_{\xi}^{g(\xi)}\left|\left(\sum_{\varphi}\langle\eta,\eta_\Omega|V_{e-ph}(\mathbf{r}_i)|\varphi,\eta_{\Omega+1}\rangle \times\langle\varphi|\mathbf{d}|\xi\rangle(E_\xi-E_\eta+\Omega_k)^{-1}+\sum_{\varphi}\langle\eta|\mathbf{d}|\varphi\rangle \times\langle\varphi,\eta_\Omega|V_{e-ph}(\mathbf{r}_i)|\xi,\eta_{\Omega-1}\rangle \times(E_\xi-E_\eta-\Omega_k)^{-1}\right)\right|_\theta^2, \tag{12}$$

where φ denotes a virtual intermediate band state; $\mathbf{d}$ is an electric dipole moment for a given optical transition. The summation was performed over all degenerated initial and final states. The notation θ denotes an averaging with respect to occupation numbers of the quasiphonon states.

Our calculations have shown that the dominant role in the corresponding electro-optic coefficients originates from the (Li–O) clusters because they give higher frequency resonances and are more sensitive to the oxygen vacancies disturbed by the Nb antisites. However, we also consider the ($Nb–O_6$) clusters and inter-the-cluster bridges in the first perturbation approach.

On the other hand, the phonons included in the electron–phonon interaction [Eq. (12)] lead to the following normal coordinates:

$$B(\Omega_k)=C_{\eta\xi}^{\gamma}(r_\lambda^\Delta)C_{\eta\xi}^{\gamma'}(r_{\lambda'}^{\Delta'})\,\mathrm{Im}\,G_{\Delta\Delta'}^{\gamma\gamma'}(r_\lambda^\Delta,\Omega_k^2) \tag{13}$$

where $G_{\Delta\Delta'}^{\gamma\gamma'}(r_\lambda^\Delta)$ is a Green function (γ and γ' are numbers of coordination sphere) defined as

$$G_{\Delta\Delta'}^{\gamma\gamma'}(r_\lambda^\Delta)=\sum_{\varphi}\left[\langle\eta|V_{e-ph}(\mathbf{r}_i)|\varphi\rangle\langle\varphi|\mathbf{d}|\xi\rangle+\langle\eta|\mathbf{d}|\varphi\rangle \times\langle\varphi|V_{e-ph}(\mathbf{r}_i)|\xi\rangle\right](E_\xi-E_\eta)^{-1}. \tag{14}$$

The resulting expression is presented below:

$$G_{\Delta\Delta'}^{\gamma\gamma'}(r_\lambda^\Delta,\Omega_k^2)=\sum_{\Omega}K_{\Delta'}^{\gamma'}(r_\lambda^\Delta)K_\Delta^\gamma(r_\lambda^\Delta)(\Omega_k^2-\Omega^2-i\delta)^{-1}, \tag{15}$$

where the coordinates $K_\Delta^\gamma(r_\lambda^\Delta)$ are obtained for a given phonon mode from the electron states averaging. To include the local lattice deformations into the Green function, we have also taken into account the (Li–O) deformation localization that allows the Dyson relation to be applied. The deformation potential and the corresponding oxygen-vacancy charge defect perturbations determine the potential operator U:

$$G_{\Delta\Delta'}^{\gamma\gamma'}(1)=G_{\Delta\Delta'}^{\gamma\gamma'}(0)+G_{\Delta\Delta'}^{\gamma\gamma'}(0)UG_{\Delta\Delta'}^{\gamma\gamma'}(1), \tag{16}$$

where $G_{\Delta\Delta'}^{\gamma\gamma'}(0)$ and $G_{\Delta\Delta'}^{\gamma\gamma'}(1)$ are Green functions for ideal and defected lattices, respectively.

Relation between real and imaginary parts of the Green function was evaluated using Kramers–Kronig dispersion relations. The main phonon contributions come from modes with relatively high frequency originating from the (Li–O) cluster. All the phonon modes were renormalized by the electron–phonon nonlinearities described above.

The contribution of the phonons to the electro-optic coefficients r_{ijk} was thus calculated using the following expression:

$$r_{ijk}^{(0,\omega)}=\frac{1}{\hbar^2}\frac{e^3N}{2!}\hat{P}_{ijk}\sum_k\sum_{\alpha,\beta}\left[\frac{\langle0|i|\alpha\rangle\langle\alpha|j|\beta\rangle\langle\beta|k|0\rangle}{(2\omega+\omega_\alpha)(\omega+\omega_\beta)} + \frac{\langle0|j|\alpha\rangle\langle\alpha|i|\beta\rangle\langle\beta|k|0\rangle}{(\omega_\alpha-2\omega)(\omega_\beta-\omega)} + \frac{\langle0|j|\alpha\rangle\langle\alpha|k|\beta\rangle\langle\beta|i|0\rangle}{(\omega+\omega_\beta)(\omega_\alpha-\omega)}\right], \tag{17}$$

where $\omega_{\alpha,\beta}$ are eigenfrequency phonon modes; $\langle\alpha|i|\beta\rangle$ are phonon mode dipole matrix elements renormalized by the electron–phonon interactions. We have performed all calculations for the phonon modes within the Γ point of the BZ. All calculated phonon modes agree well with the experimen-

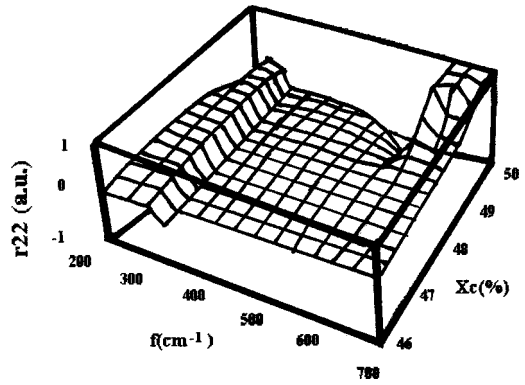

FIG. 6. Ionic (phonon) contribution to the electro-optic coefficient r_{22} as calculated from Eq. (17).

tal data obtained in Ref. 6. The calculations presented allow the changes in the electro-optics coefficients to be detected with precision up to 0.2 pm/V.

At the beginning the calculations of the electro-optic coefficients were carried out separately for the harmonic phonon modes then we superimposed phonon modes renormalized by the electron–phonon interactions. Contributions of each phonon mode to calculated electro-optic coefficient were determined for crystals with various compositions X_c. The corresponding results are shown in Fig. 6.

One can see the opposite signs of contributions to the electro-optic coefficient r_{22} arising from various phonon modes. Most of the active phonon modes have positive sign contributions whereas the modes higher than 580 cm^{-1} give opposite negative contributions which drastically increase with the parameter X_C. This one proves that Li–O dipole plays an important role in the large value of the EO coefficient r_{22} obtained in the stoichiometric crystal.[26]

The physical origin of the opposite sign contributions can be attributed to different directions of the noncentrosymmetry within the Nb–O and Li–O shells.

V. INFLUENCE OF THE INTRINSIC NONSTOICHIOMETRY ON A DISPERSION OF THE ELECTRO-OPTICS COEFFICIENTS

The calculations of the electronic part of the electro-optic tensors have been carried out using the similar expression and the calculation techniques similar to previous works:[8,22]

$$\chi_{ijk}^{(\omega,\omega)}=\frac{1}{\hbar^2}\frac{e^3N}{2!}\hat{P}_{ijk}\sum_{k}\sum_{\alpha,\beta}\left[\frac{\langle 0|i|\alpha\rangle\langle\alpha|j|\beta\rangle\langle\beta|k|0\rangle}{(2\omega+\omega_\alpha)(\omega+\omega_\beta)}+\frac{\langle 0|j|\alpha\rangle\langle\alpha|i|\beta\rangle\langle\beta|k|0\rangle}{(\omega_\alpha-2\omega)(\omega_\beta-\omega)}+\frac{\langle 0|j|\alpha\rangle\langle\alpha|k|\beta\rangle\langle\beta|i|0\rangle}{(\omega+\omega_\beta)(\omega_\alpha-\omega)}\right], \tag{18}$$

where the $\langle\alpha|i|\beta\rangle$ are dipole matrix momenta between the α and β electronic band states; P is a permutation operator; N is a concentration of the valence electrons; the summation over **k** indicates summation over the whole effective Brillouin zone.

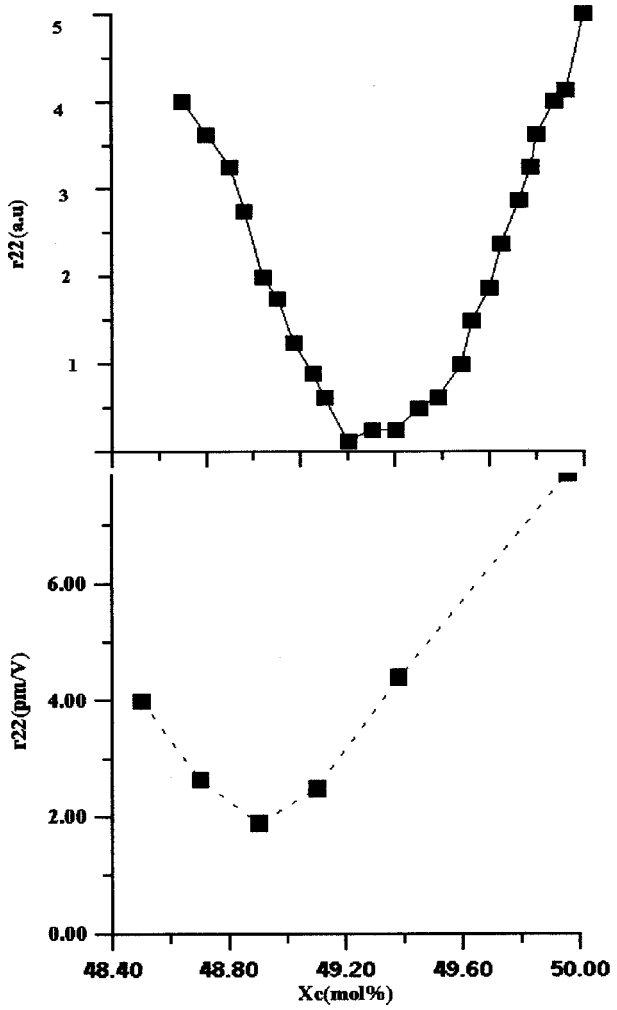

FIG. 7. Spectral dependence of the r_{33} vs X_C.

For comparison we have added the spectral dependence of the r_{33} electro-optic tensor component versus the X_C (see Fig. 7). One can see absence of the minimum in the appropriate dependencies for the electro-optics coefficients that was observed for the r_{22}. The origin of this phenomenon may be caused by a specific anisotropy of electron–phonon interaction in the corresponding electro-optics coefficients.

Comparing the experimental data with the theoretically calculated (see Fig. 8) one can see a good agreement. The developed approach is valuable for simulation of the changes of the electro-optics coefficients versus the nonstoichiometry parameters X_C. However to determine the absolute values of

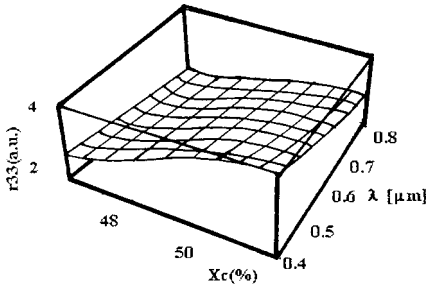

FIG. 8. Comparison between the calculated and experimental behaviors in the composition dependence of the EO coefficient r_{22}.

the r_{222} tensor components the precision of the dipole moment's evaluations should be enhanced. At the same time changes of the r_{222} tensor components give more important information for the technologists showing simultaneously the main directions of the electro-optics coefficient changes.

VI. CONCLUSIONS

In the present work the band structure approach with a simultaneous molecular dynamics structure optimization procedure seems to be sufficient for explaining of the main features in the nonstoichiometry-spectral-dependent behaviors of the r_{ijk} electro-optic linear coefficients. An appearance of the minimum in the r_{22} electro-optic coefficients is caused by a competition between the long-range order $2p$ O$-2s$ Li band contributions disturbed by the oxygen vacancies and the localized $3d$ Nb$-2p$ O cluster fragments. Molecular dynamics methods unambiguously show an occurrence of a correlation between the band states behaviors (optical oscillators at 4.8 and 6.82 eV) and charge density noncentrosymmetry for the particular (Nb$-$O$_6$) clusters. Inclusion of the phonon subsystem shifts the position of the r_{222} closely to the experimental ones. However, several discrepancies remain for the values of the particular depth. In our opinion this problem can be resolved in future by introduction of the intercluster fragments and taking into account of the higher order anharmonic interactions and new cluster configurations determining the absolute value of the electro-optic coefficient r_{22}. An essential influence of near-the-defect oxygen on the noncentrosymmetry of the electrostatic potential is shown. The electronic part of the (Nb$-$O) clusters gives more than 50% contribution to the total output electro-optic coefficient r_{22}. One can also see absence of the minimum in the corresponding dependencies for the r_{33}. The origin of this phenomenon may be caused by a specific anisotropy of electron$-$phonon interaction in the particular electro-optics tensor components. The phonon subsystem considerably increases its contribution to r_{22} within the $X_C = 48.4\% - 48.8\%$.

[1] U. Schlarb and K. Betzler, Phys. Rev. B **48**, 15613 (1993).
[2] F. Abdi, M. Aillerie, P. Bourson, M. D. Fontana, and K. Polgar, J. Appl. Phys. **84**, 2251 (1998); H. Donnerberg, *Atomic Simulation of Electro-Optic and Magneto-Optic Oxide Materials* (Springer, Berlin, 1999), p. 33.
[3] U. Schlarb and K. Betzler, Phys. Rev. B **50**, 751 (1994).
[4] M. Wohleke, G. Corradi, and K. Betzler, Appl. Phys. B: Lasers Opt. **63**, 323 (1996).
[5] L. Kovacs, G. Ruschhaupt, K. Polgar, G. Corradi, and M. Wohleke, Appl. Phys. Lett. **70**, 2801 (1997).
[6] A. Ridah, P. Bourson, M. D. Fontana, and G. Malovichko, J. Phys.: Condens. Matter **9**, 9697 (1997).
[7] E. H. Turner, F. R. Nash, and P. M. Bridenbouigh, J. Appl. Phys. **42**, 4155 (1971).
[8] I. V. Kityk, Phys. Solid State **33**, 1026 (1991).
[9] I. V. Kityk and B. Sahraoui, Phys. Rev. B **60**, 942 (1999).
[10] B. Sahraoui, I. V. Kityk, P. X. Phu, P. Huddhomme, and A. Gorgues, Phys. Rev. B **59**, 9229 (1999).
[11] I. V. Kityk, J. Kasperczyk, and B. V. Andrievskii, Phys. Lett. A **216**, 161 (1996).
[12] M. Malachowski, I. R. Kityk, and B. Sahraoui, Phys. Status Solidi **207**, 405 (1998).
[13] I. V. Kityk, I. N. Yaszczishin, and L. V. Tyagnyriadko, Glass Phys. Chem. **20**, 404 (1994).
[14] E. Golis, I. V. Kityk, J. Kasperczyk, and J. Wasylak, Mater. Res. Bull. **9**, 1057 (1996).
[15] W. Y. Ching, Z.-Q. Gu, and Y.-N. Xu, Phys. Rev. B **50**, 1992 (1994).
[16] I. V. Kityk, Ukr. Phys. J. **32**, 678 (1990).
[17] G. B. Bachelet, D. R. Hamann, and M. Schluter, Phys. Rev. B **26**, 4199 (1982).
[18] Ya. O. Dovgii, I. V. Kityk, A. O. Matkovskii, D. Yu. Sugak, and S. B. Ubizskii, Phys. Solid State **34**, 575 (1992); S. V. Gorbunov and Y. M. Krushalov, *ibid.* **41**, 539 (1999).
[19] I. V. Kityk, Optics and Lasers in Engineering Vol. 35 (2001), p. 239.
[20] P. Hohenberg and W. Kohn, Phys. Rev. **136**, 864 (1964).
[21] I. V. Kityk and E. Jakubczyk, Appl. Opt. **38**, 5162 (1999).
[22] I. V. Kityk, B. Sahraoui, P. X. Nguyen, G. Rivoire, and J. Kasperczyk, Nonlinear Opt. **18**, 13 (1997).
[23] J. B. Perdew and A. Zunger, Phys. Rev. B **23**, 5048 (1981).
[24] D. M. Ceperley and B. J. Adler, Phys. Rev. Lett. **45**, 161 (1980).
[25] D. J. Chadhi and M. L. Cohen, Phys. Rev. B **8**, 5747 (1973).
[26] A. D. Becke, J. Chem. Phys. **98**, 1372 (1994); **98**, 5648 (1994); D. E. Woon and T. H. Dunning, *ibid.* **98**, 1358 (1993).
[27] H. Kusen, *Mathematical Approach Calculations for PC* (Elsevier, Amsterdam, 1996), p. 156.